

**UCC Library and UCC researchers have made this item openly available.  
 Please [let us know](#) how this has helped you. Thanks!**

<b>Title</b>	Motion and performance of BBDB OWC wave energy converters: I, hydrodynamics
<b>Author(s)</b>	Sheng, Wanan
<b>Publication date</b>	2019-01-04
<b>Original citation</b>	Sheng, W. (2019) 'Motion and performance of BBDB OWC wave energy converters: I, hydrodynamics', Renewable Energy. doi:10.1016/j.renene.2019.01.016
<b>Type of publication</b>	Article (peer-reviewed)
<b>Link to publisher's version</b>	<a href="http://www.sciencedirect.com/science/article/pii/S0960148119300163">http://www.sciencedirect.com/science/article/pii/S0960148119300163</a> <a href="http://dx.doi.org/10.1016/j.renene.2019.01.016">http://dx.doi.org/10.1016/j.renene.2019.01.016</a> Access to the full text of the published version may require a subscription.
<b>Rights</b>	© 2019, Elsevier Ltd. All rights reserved. This manuscript version is made available under the CC BY-NC-ND 4.0 license. <a href="https://creativecommons.org/licenses/by-nc-nd/4.0/">https://creativecommons.org/licenses/by-nc-nd/4.0/</a>
<b>Embargo information</b>	Access to this article is restricted until 24 months after publication by request of the publisher.
<b>Embargo lift date</b>	2021-01-04
<b>Item downloaded from</b>	<a href="http://hdl.handle.net/10468/7279">http://hdl.handle.net/10468/7279</a>

Downloaded on 2021-11-27T07:13:40Z

# Accepted Manuscript

Motion and performance of BBDB OWC wave energy converters: I, hydrodynamics

Wanan Sheng

PII: S0960-1481(19)30016-3

DOI: <https://doi.org/10.1016/j.renene.2019.01.016>

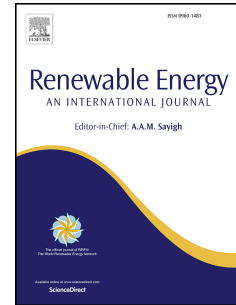
Reference: RENE 11017

To appear in: *Renewable Energy*

Received Date: 26 February 2018

Revised Date: 23 December 2018

Accepted Date: 3 January 2019



Please cite this article as: Sheng W, Motion and performance of BBDB OWC wave energy converters: I, hydrodynamics, *Renewable Energy* (2019), doi: <https://doi.org/10.1016/j.renene.2019.01.016>.

This is a PDF file of an unedited manuscript that has been accepted for publication. As a service to our customers we are providing this early version of the manuscript. The manuscript will undergo copyediting, typesetting, and review of the resulting proof before it is published in its final form. Please note that during the production process errors may be discovered which could affect the content, and all legal disclaimers that apply to the journal pertain.

# **Motion and performance of BBDB OWC wave energy converters: I, Hydrodynamics**

**Wanan Sheng**

Centre for Marine and Renewable Energy Ireland (MaREI), Environmental Research Institute,  
University College Cork, Ireland. Email: [w.sheng@ucc.ie](mailto:w.sheng@ucc.ie)

# Motion and performance of BBDB OWC wave energy converters: Hydrodynamics

Wanan Sheng

SW Mare Maine Technology

Email: wanan\_sheng@outlook.com

## ABSTRACT

The Backward Bent Duct Buoy (BBDB) oscillating water column (OWC) wave energy converter (WEC) has been invented following the so-far most successful OWC navigation buoys in wave energy utilisation, with aims to build large and efficient OWC wave energy converters for massive wave energy production. The BBDB device could use its multiple motion modes to enhance wave energy conversion, however, the mechanism of the motion coupling and their contributions to wave energy conversion have not been well understood in a systematic manner. In particular, the numerical modelling has been very limited in exploring how these motions are coupled and how the wave energy conversion capacity can be improved.

As in this part of the research of a systematic study using numerical modelling, focus is on the understanding of the hydrodynamic performance for the BBDB OWC wave energy converter. In the study, the boundary element method based on potential flow theory has been applied to calculate the basic hydrodynamic parameters for the floating BBDB OWC structure and the water body in the water column in the BBDB OWC device. With the calculated hydrodynamic parameters and the decoupled and coupled models for the BBDB OWC dynamics, it is possible to examine these hydrodynamic parameters in details and to understand how they interact each other and how they contribute to the relative internal water surface motion, a most important response in terms of wave energy conversion of the OWC devices. All these will provide a solid base for further studying the power performance of the BBDB devices for converting energy from waves as shown in the second part of the research.

**Keywords:** Wave energy converter; oscillating water column; backward bent duct buoy (BBDB); frequency-domain analysis; hydrodynamic performance; wave energy conversion

## 25 1 INTRODUCTION

26 Wave energy is well known to have a potential to contribute to the renewable energy mix in future and  
27 remains one of the largest untapped renewable resources so far since the technologies are not matured  
28 enough for efficiently, reliably and economically extracting energy from sea waves [1, 2]. Researchers  
29 and developers have made great efforts in advancing wave energy technologies since 1799 when a French  
30 father and son filed a patent for their wave energy device and more than a thousand of wave energy  
31 technologies have been patented (see [3]). To date, the most successful story for wave energy utilisation  
32 would be the navigation buoys powered by wave energy, which were invented and developed by a  
33 Japanese, Yoshio Masuda, since 1940s, a pioneer in modern wave energy technologies. The developed  
34 navigation buoys were very successful: 700 buoys have been used in Japan, while other 500 have been  
35 sold to the other countries including 20 in the United States [4]. Based on the current terminology of wave  
36 energy technologies, those navigation buoys are in fact the oscillating water columns (OWCs).  
37 Interestingly, the OWC wave energy converters were first called the Masuda devices following the  
38 inventor's name, and much later named as oscillating water column as we used formally now, according  
39 to Ross [5]. Though it is not very clear when the name is firstly used, the references the author searched  
40 show that Evans used it in 1978 when he first formulated the relevant mathematical equations for the  
41 hydrodynamics of OWCs [6]. Though very successful in those OWC navigation buoys, Masuda had  
42 further worked on the OWC energy conversion principle, aiming to build large and efficient OWC wave  
43 energy converters for massive wave energy production, that is, first 'Kaimei' [7] and then Backward Bent  
44 Duct Buoy (BBDB) [4]. As a unique advantage for the OWC devices as pointed out by Evans [8], they  
45 may be the only wave energy converters which can effectively overcome the challenges for converting  
46 the low-frequency motion in waves ( $\sim 0.1$  Hz) into electricity of 50 or 60 Hz.

47 OWC wave energy converters are now being regarded as one of the most promising wave energy  
48 converters, and probably the most practical and reliable wave energy converters due to their inherent  
49 wave energy conversion principle. It is interesting to see that the most recent European Wave and Tidal  
50 Energy Conference (EWTEC 2017) (Cork, Ireland) (<http://www.ewtec.org/ewtec-2017/>) has shown a  
51 significantly increased interest in OWC wave energy technologies. While many other wave energy  
52 converters utilise the low-speed motion of the device structure(s) or water body (thus large forces) for  
53 direct power conversion, OWC wave energy converters employ the air flow driven by the internal water  
54 surface (IWS) motion (the relative motion between the structure and the water body in the water column)  
55 in the water column of the OWC devices. In the OWC power conversion from pneumatic power to  
56 mechanical power, the air flow driven by the IWS motion is normally accelerated by many times (roughly  
57 at 50-150 times [9]), and the accelerated air flow could drive the air turbine Power Take-offs (PTOs) in

58 high rotational speeds (up to 3000 rpm for the Wells turbines and 1500 rpm for impulse turbines [10]).  
59 This high rotational speed of the PTO system allows a low torque acting on the PTOs when compare to  
60 the direct conversion in many other wave energy technologies, and thus it is very beneficial for a high  
61 reliability in the OWC PTO and the other relevant components (including the structure of the device) in  
62 terms of a long-term wave energy production. This energy conversion principle is very analogous to the  
63 conventional power stations, where the steam turbines have a very high rotational speed, normally at  
64 3000rpm or 3600 rpm (50Hz or 60Hz), hence allowing small torques acting the steam turbines, allowing a  
65 very high reliability in long-term energy production.

66 Currently, some OWC technologies have been progressed to high level of technology readiness levels,  
67 and a few of them even to practical wave energy plants/devices. The shoreline plants include LIMPET  
68 [11, 12], PICO [13, 14], Mutriku [15, 16] and the floating OWC devices includes the BBDB OE Buoy [17,  
69 18]. It has been reported that the LIMPET OWC plant has generated electricity to the grid for more than  
70 60,000 hours in a period of about 10 years [19], whilst OceanEnergy Ltd have sea-trialled their 1/4 scaled  
71 'Back Bent Duct Buoy (BBDB)' in Galway Bay (Ireland) for more than 3 years [18]. At the time of  
72 writing this article, OceanEnergy Ltd are in the process of manufacturing a full scale OE buoy and are  
73 planning to undergo an open-sea trial in the open sea in Hawaii, US, in near future. In addition, a recent  
74 research report by the EU Joint Research Centre (JRC) [2] has shown that the current capacity factors  
75 achieved 25 % in the case of OWC wave energy converters and 10 % for other device types (capacity  
76 factor is defined as the ratio of the actual annual output of energy production divided by the rated power  
77 of the device and the hours of the year). Also in [2], the capacity factor for the economically viable ocean  
78 energy production is recommended at 30% - 40%. In this regard, OWC wave energy converters may be  
79 the wave energy technology which has a very close capacity factor level to the requirement.

80 To assess and optimise the hydrodynamic and power performance of the OWC devices, numerical  
81 methods and experimental methods both are important and have been used widely. Since Evans firstly  
82 formulated the theory for OWC devices in 1978 [6], numerical methods have been advanced a great deal,  
83 and both analytical and numerical models have been proposed and used [6, 9, 20-24]. Currently, two  
84 distinguishing methods in mathematical/numerical modelling are used for studying the OWC  
85 performance. The first approach is called the massless piston model [6, 25] for which the internal water  
86 surface (IWS) in the water column is taken as a massless rigid piston (a zero-thickness structure), and the  
87 motion of the internal water surface is solved together with other hydrodynamic parameters. A slightly  
88 different version of the massless piston model is a two-body system for the OWCs [9, 24, 26], in which  
89 the first rigid body is the device itself whilst the second rigid body is an imaginary piston (with a length)  
90 for replacing the internal water surface in the water column. In the latter method, when a PTO is applied

91 and coupled into the dynamic system, the pressure and the thus modified internal water surface in the air  
92 chamber can be solved using the coupling of the hydrodynamics and thermodynamics for the OWC  
93 devices (see [27]).

94 The second approach is the pressure distribution model [21], in which on the internal water-surface the  
95 dynamic air pressure is distributed [22, 28, 29]. In the numerical modelling, a reciprocity relation must be  
96 employed as shown by Falnes [30] such that the conventional boundary element methods (BEMs) can be  
97 used accordingly.

98 In linear cases, the two methods mentioned above can be only different when the higher-order motions in  
99 the water column are considered, and it is believed that the pressure distribution method is more suitable  
100 for accommodating the high-order motions in the water column [29]. However, for the purpose wave  
101 energy conversion, the heave motions account only. The higher-order motions do not contribute to the net  
102 wave energy conversion, and thus can be excluded in the analysis as it does in this research. A point  
103 should be noted here that in the OWCs with nonlinear air turbine PTOs, the numerical and experimental  
104 data have both shown that the pressures in the air chamber in OWC devices are much more nonlinear than  
105 that of the IWS motions. In this regard, solving the IWS motion first in the hydrodynamic module is more  
106 reasonable since the frequency-domain potential flow theory can not handle the nonlinear motions and  
107 forces.

108 As one type in the floating OWCs, the backward bent duct buoy (BBDB) OWC attracted a lot of interest  
109 from both researchers and developers since it was first shown by Masuda in 1987 [4]. Due to its unique  
110 design, the BBDB OWC devices could use its multiple motion modes to enhance the device power  
111 performance. This implies a more complicated hydrodynamic couplings among the motions and has made  
112 the numerical studies more difficult. As a result of such difficulties, the BBDB hydrodynamic and power  
113 performance are found to be difficult to be optimised because the strong interactions among the multiple  
114 motion modes, namely, surge, heave and pitch motions of the structure, as well as the internal water  
115 motion. This is why limited attempts have been made using numerical models for the BBDB converters  
116 [28, 31-33], and a systematic study on the hydrodynamics and thus the optimisations on the BBDB OWC  
117 devices have not been carried out effectively.

118 To streamline the development and provide the reference wave energy converters, National Renewable  
119 Energy Laboratory (NREL) and Sandia National Laboratory under the US DoE financial support have  
120 established the reference models for marine renewable energy (wave and tidal energy [34]). A BBDB has  
121 been chosen as one of three reference wave energy converters, named RM6 [23] (other two are: floating  
122 point absorber, RM3 and the bottom-fixed oscillating surging wave energy converter, RM5, see [35]). In

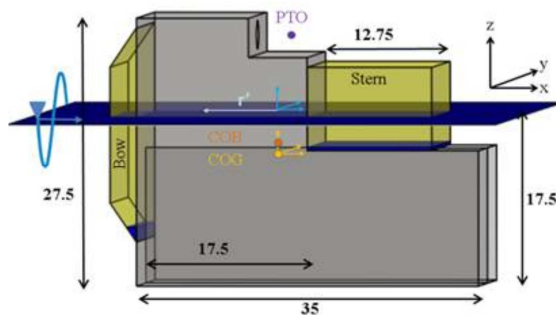
123 this research, a systematic study on the reference BBDB OWC is aimed to provide better understanding to  
 124 its hydrodynamic and power performance.

125 In this research, focus is on the hydrodynamics of the RM6 BBDB, including some basic issues with the  
 126 numerical convergence, coupling and decoupling of the motions and most importantly, how to identify  
 127 and how to optimise the device so that an improved device would have better motion performance for  
 128 more efficient wave energy conversion. The work is arranged as follows: in Section 2, the RM6 model is  
 129 briefly introduced, together with a short description of panels used for the numerical modelling; Section 3  
 130 gives the introduction to the methodologies used in this study; in Section 4, a validation is made using the  
 131 available published data, while Section 5 gives the approaches for improving hydrodynamic and power  
 132 performance. The conclusions are drawn in Section 6.

## 133 2 RM6 REFERENCE MODEL

134 Reference Model 6 (RM6) is a Backward Bent Duct Buoy (BBDB) oscillating water column wave energy  
 135 converter, which was designed as part of the DOE sponsored Reference Model Project [35] (see Figure 1).  
 136 The BBDB has a horizontal water column of 35m long, 14m high and 27m wide and a vertical water  
 137 column of an area of 17.5m\*27m (472.5m<sup>2</sup>).

138 To study the BBDB OWC device, the panels/patches used in numerical modelling can be seen in Figure 2.  
 139 The coordinate origin for studying the motions and forces on this particular OWC device is located at the  
 140 centre of the free surface in the water column (see Figure 2), with x-y plane on the calm water surface,  
 141 and z-axis pointing up. This approach could simplify the motion and the force analysis and avoid the  
 142 manipulations of the motion and force transformation (from the centre of gravity to the centre of free  
 143 surface in the water column). In the chosen coordinate, the translational motions (named the motions  
 144 along x-axis, y-axis and z-axis, respectively) will be different from those at the centre of gravity (named  
 145 formally surge, sway and heave). However, for a purpose of simplification, the translational motions at  
 146 the chosen coordinate will be still called as surge, sway and heave in the following analysis.

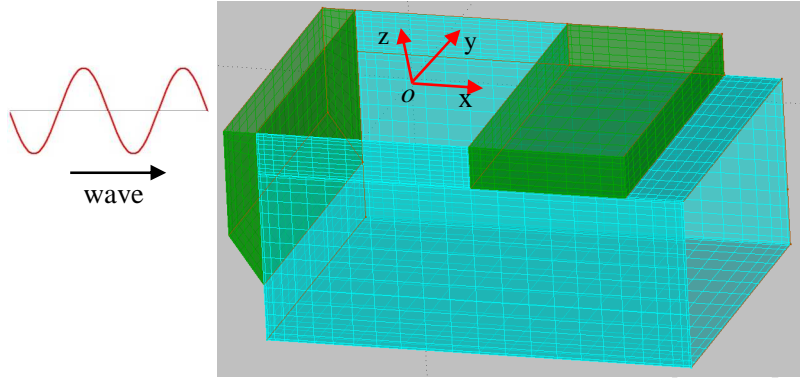


147



148

Figure 1 RM6 design model (from [23])



149

150 Figure 2 Panels on RM6 for hydrodynamic analysis (green: solid surfaces, Cyan: panels for thin structures)

151 The matrix for inertia is defined by following the WAMIT manual [36],

$$M = \begin{bmatrix} m & 0 & 0 & 0 & mz_g & -my_g \\ 0 & m & 0 & -mz_g & 0 & mx_g \\ 0 & 0 & m & my_g & -mx_g & 0 \\ 0 & -mz_g & my_g & I_{11} & I_{12} & I_{13} \\ mz_g & 0 & -mx_g & I_{21} & I_{22} & I_{23} \\ -my_g & mx_g & 0 & I_{31} & I_{32} & I_{33} \end{bmatrix} \quad (1)$$

152 where  $m$  is the mass,  $(x_g, y_g, z_g)$  are the coordinates of the centre of gravity in the body coordinate system.

153 The moments of inertia are defined are given in Newman's book ([37], p307), as

$$\begin{cases} I_{11} = \iiint_V (y^2 + z^2) dm_0 \\ I_{22} = \iiint_V (x^2 + z^2) dm_0 \\ I_{33} = \iiint_V (x^2 + y^2) dm_0 \\ I_{12} = I_{21} = -\iiint_V xy dm_0 \\ I_{13} = I_{31} = -\iiint_V xz dm_0 \\ I_{23} = I_{32} = -\iiint_V yz dm_0 \end{cases} \quad (2)$$

154 where  $V$  represents the whole volume of the structure, and  $dm_0$  the distributed mass of the structure.155 Based on the structure as above, the device has a displacement of  $1995.84 \text{ m}^3$ , and the radii of moments of

156 inertia at the centre of gravity are given in Table 1.

157

Table 1 Radii of the moment of inertia (taken from [23])

$R_{xx} = 12.53\text{m}$	$R_{xy} = 0\text{m}$	$R_{xz} = 3.35\text{m}$
--------------------------	----------------------	-------------------------

$R_{yx} = 0\text{m}$	$R_{yy} = 14.33\text{m}$	$R_{yz} = 0\text{m}$
$R_{zx} = 3.35\text{m}$	$R_{zy} = 0\text{m}$	$R_{zz} = 14.54\text{m}$

### 158 3 METHODOLOGIES

159 In this research, the two-body system is used, with the structure of the BBDB device being taken as the  
 160 first body and the piston for replacing the water body in the water column as the second body. The  
 161 motions and forces will be calculated based on the chosen coordinate (see above), with the centre of  
 162 gravity of the structure at (5.16m, 0, -4.29m) [23].

#### 163 3.1 Two-body system

164 Considering the BBDB wave energy converter, it may experience 6 DOF motions in waves. In the body  
 165 coordinate, only the heave motions of the structure and the piston, more specifically, their relative motion  
 166 contributes for pneumatic power conversion. However, since the complicated structure, both heave  
 167 motions may be strongly coupled with other motion modes. Hence for a completion, following motion  
 168 modes must be included in the dynamic equation, with 6-DOF motions for the structure and one motion  
 169 mode for the piston. The other motion modes for the piston are ignored because the piston can be taken as  
 170 a very thin structure, hence they could not contribute to the dynamic system. For this reason, the heave  
 171 motion of the piston is re-defined as motion mode No. 7 for a convenience in the following analysis):

- 172  $X_1$ : surge motion of the structure;
- 173  $X_2$ : sway motion of the structure;
- 174  $X_3$ : heave motion of the structure;
- 175  $X_4$ : roll motion of the structure;
- 176  $X_5$ : pitch motion of the structure;
- 177  $X_6$ : yaw motion of the structure;
- 178  $X_7$ : heave motion of the 'imaginary piston'.

179 In the frequency domain, the dynamic equation for the RM6 BBDB OWC with an air turbine PTO in  
 180 waves can expressed as

$$\begin{pmatrix} a_{11} & a_{12} & a_{13} & a_{14} & a_{15} & a_{16} & a_{17} \\ a_{21} & a_{22} & a_{23} & a_{24} & a_{25} & a_{26} & a_{27} \\ a_{31} & a_{32} & a_{33} & a_{34} & a_{35} & a_{36} & a_{37} \\ a_{41} & a_{42} & a_{43} & a_{44} & a_{45} & a_{46} & a_{47} \\ a_{51} & a_{52} & a_{53} & a_{54} & a_{55} & a_{56} & a_{57} \\ a_{61} & a_{62} & a_{63} & a_{64} & a_{65} & a_{66} & a_{67} \\ a_{71} & a_{72} & a_{73} & a_{74} & a_{75} & a_{76} & a_{77} \end{pmatrix} \begin{pmatrix} X_1 \\ X_2 \\ X_3 \\ X_4 \\ X_5 \\ X_6 \\ X_7 \end{pmatrix} = \begin{pmatrix} F_1 \\ F_2 \\ F_3 + pA_0 \\ F_4 \\ F_5 \\ F_6 \\ F_7 - pA_0 \end{pmatrix} \quad (3)$$

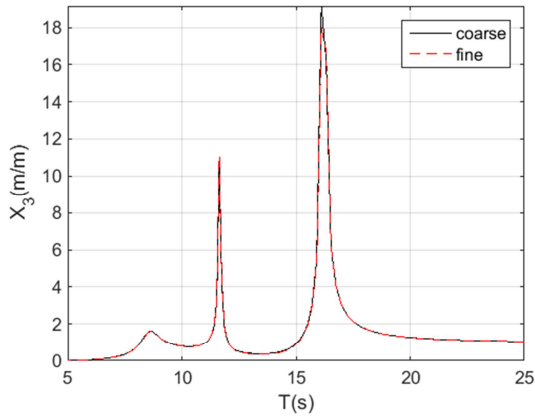
181 with

$$a_{jk} = -\omega^2 (M_{jk} \delta_{jk} + A_{jk}) + i\omega (B_{jk} + B_{jk}^{vis}) + C_{jk} \quad (j, k=1, \dots, 7) \quad (4)$$

182 where  $\delta_{jk}=1$  when  $j=k$  and  $\delta_{jk}=0$  ( $j \neq k$ );  $M_{ij}=M_j$  is the corresponding mass or moment of inertia of the  
 183 bodies based on the motion modes as defined as above;  $A_{jk}$ ,  $B_{jk}$  and  $C_{jk}$  are the added mass, radiated  
 184 damping coefficients and the restoring coefficients;  $B_{jk}^{vis}$  is the linear viscous damping coefficient;  $X_j$  the  
 185 complex motion amplitude of the corresponding motion mode;  $F_j$  the complex excitation;  $p$  the complex  
 186 chamber gauge pressure (note: the positive pressure in the air chamber will increase the heave motion of  
 187 the structure, and reduce the heave motion of the piston. In the case without a PTO, the chamber pressure  
 188  $p=0$ ); and  $A_0$  the sectional area of the water column at water plane.

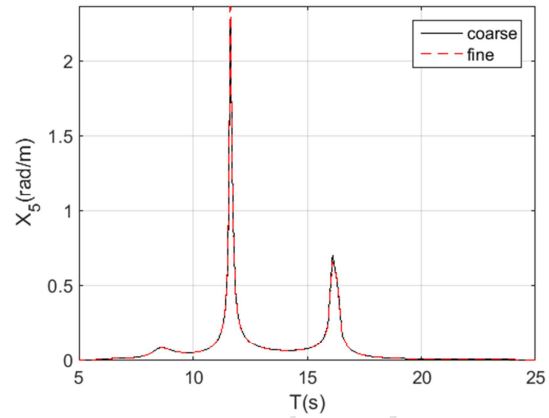
### 189 3.2 Numerical convergence

190 In this numerical modelling, the higher-order panel method is used in the BEM analysis (see [36]). By  
 191 controlling the relevant parameters in the numerical modelling, the number of unknowns in linear  
 192 dynamic system can be different for studying the numerical convergence. In the comparisons, the  
 193 unknowns solved in the linear system are 1788 for the fine panels and 1258 for the coarse panels,  
 194 respectively. For these two quite different panels, the RAOs of the motions are almost identical, with  
 195 some very small differences at the peaks. This confirms that the convergence of the numerical modelling  
 196 has been well achieved and gives the confidence to obtain the relevant hydrodynamic parameters for  
 197 further analyses.



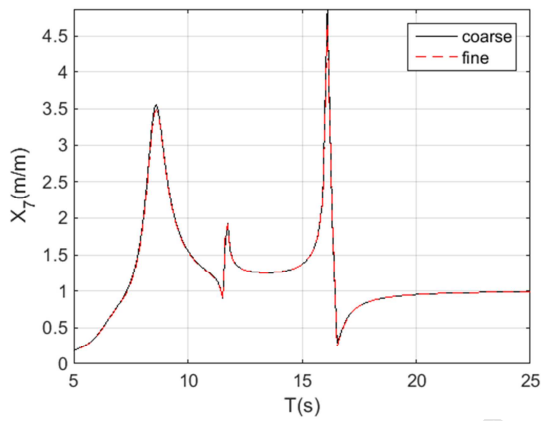
198

(a) Heave RAO (structure)



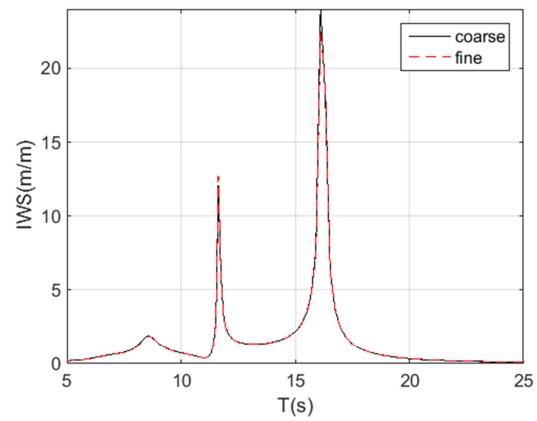
199

(b) Pitch RAO



200

(c) Heave RAO ('piston')



201

(d) Relative motion RAO

202

Figure 3 RAO comparisons for cases of different panels

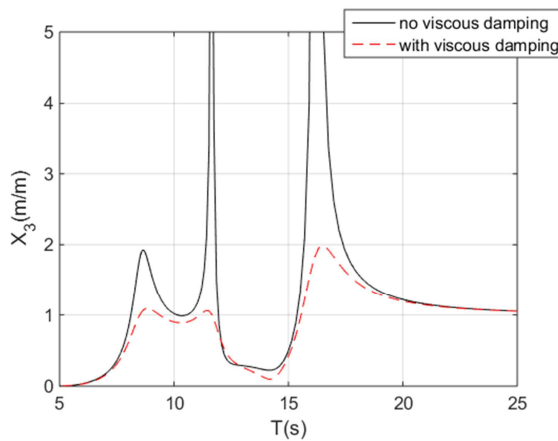
### 203 3.3 Linear viscous damping

204 In the boundary element method, only the damping from the radiated wave is included. In reality, other  
 205 types of damping may exist, for instance, damping from the viscosity of the water. In this study, a linear  
 206 viscous damping is adopted by following Bull [28], with a form as

$$B_{jj}^{vis} = 0.04 \sqrt{(m_{jj} + A_{jj})} C_{jj} \quad (j=1, \dots, 7) \quad (5)$$

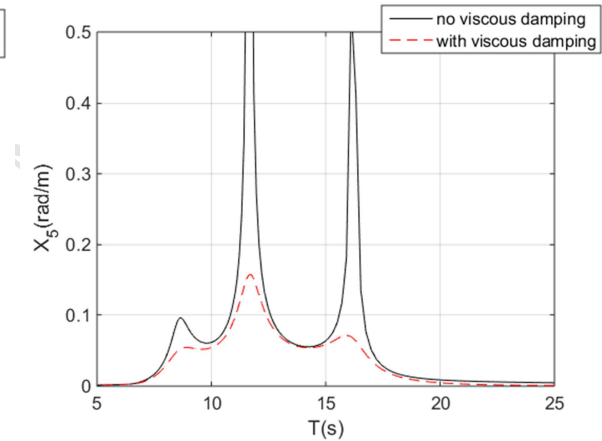
207 This is a generic linear viscous damping coefficient expression, usable for general purposes. However, for  
 208 specific wave energy converters, the linear viscous damping coefficients may be needed to be adjusted for  
 209 a better representation of the effect of viscous damping, depending on the practical design of the wave  
 210 energy converters.

211 The choice of the additional linear damping is for two reasons: the first reason is that the additional linear  
 212 damping could allow the frequency domain analyses, which could simplify the dynamic problem  
 213 significantly; and the second reason is that the application of the additional linear damping could limit the  
 214 motion responses within an acceptable range as those nonlinear additional damping coefficients, although  
 215 these linear additional damping coefficients may be only applicable for a certain limited motion amplitude.  
 216 With the added linear viscous damping ('with viscous damping' in the figures), the RAOs are much more  
 217 acceptable when compared to the RAOs without viscous damping ('no viscous damping'). The RAOs of  
 218 heaves (structure and piston), piston and the internal water surface ('IWS' in the figure) with the given  
 219 additional damping shown in Eqs. (5) and the RAOs without additional damping coefficients are  
 220 compared in Figure 4. It can be seen that with the additional damping coefficients, the maximal RAOs of  
 221 the heave and IWS motions are more acceptable. For instance, the maximal heave RAO is about or less  
 222 than 2 both for the structure and for the piston, and the relative motion of the water body in the water  
 223 column is less 3.



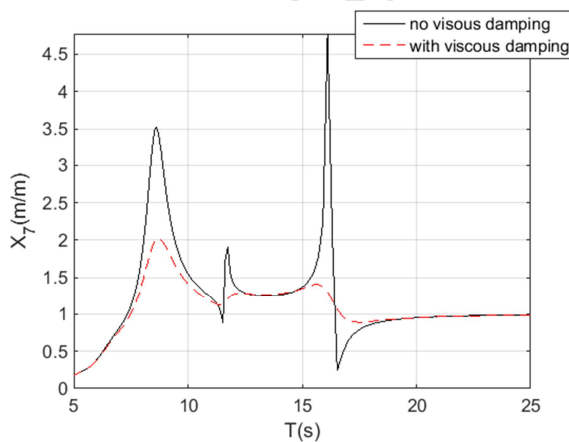
224

(a) Heave RAOs (structure)

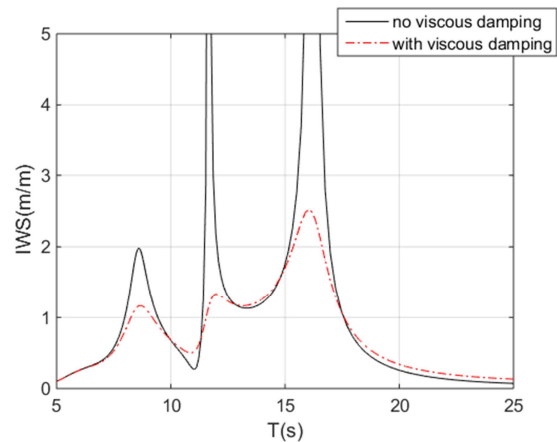


225

(b) Piston RAOs (structure)



226



227 (c) Heave RAOs (piston) (d) Relative RAOs

228 *Figure 4 RAOs of motions with and without linear viscous damping*

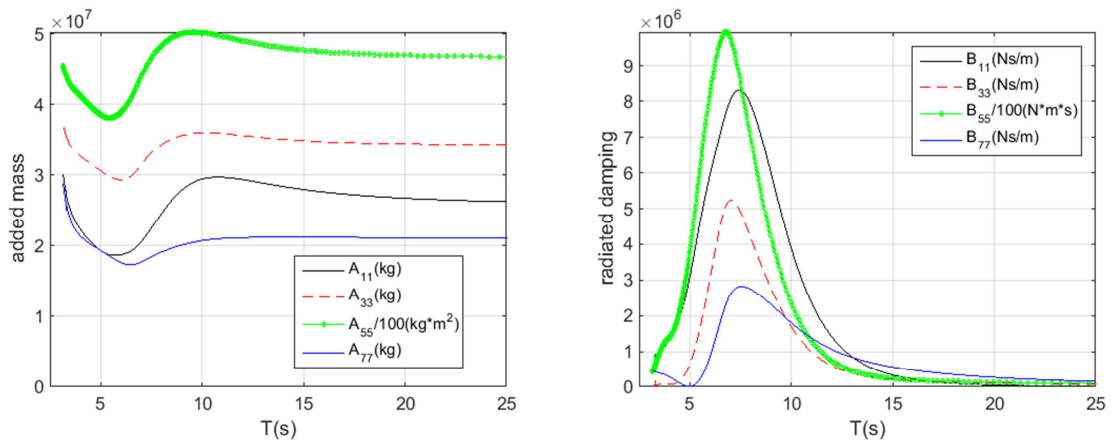
### 229 3.4 Added mass and damping coefficients (radiated)

230 To examine the couplings between the motion modes in the RM6 BBDB OWC wave energy converter, its  
 231 added mass and damping coefficients for both self- and cross- terms have been studied in an incident  
 232 angle  $45^\circ$  of the waves, such a wave direction that all couplings between motion modes can be easily  
 233 sorted out.

#### 234 3.4.1 Self-radiated added mass and damping coefficients

235 The self-radiated added mass and damping coefficients are important in the dynamic system, and  
 236 generally they are frequency-dependent. Figure 5 shows all these curves: added mass and damping  
 237 coefficients are both similar in shapes (Figure 5a and Figure 5b for added mass and damping coefficients  
 238 respectively), but the magnitudes of the RAOs can be very different. For instance, the added moment of  
 239 inertia and the damping coefficient for pitch have much larger values (in the figures their values are  
 240 reduced by 100 times for better comparisons). The added masses have the most frequency-dependent  
 241 values in the short wave periods from 2-10s, but asymptote to constants at large waver periods. The  
 242 damping coefficients have normally maximal values between 7-8s, and asymptote to zero at both zero  
 243 wave period and frequency. Obviously, the maximal damping coefficients are be very different for  
 244 different motion modes.

245 From Figure 5, it can be seen that all the self-radiated added masses and damping coefficients are positive.



246 (a) Self-radiated added mass/moment of inertia

(b) Self-radiated damping coefficients

248 *Figure 5 Added mass for different motion modes (note: added moment of inertia and radiated damping coefficient*  
 249 *for pitch have been divided by 100 for better comparisons)*

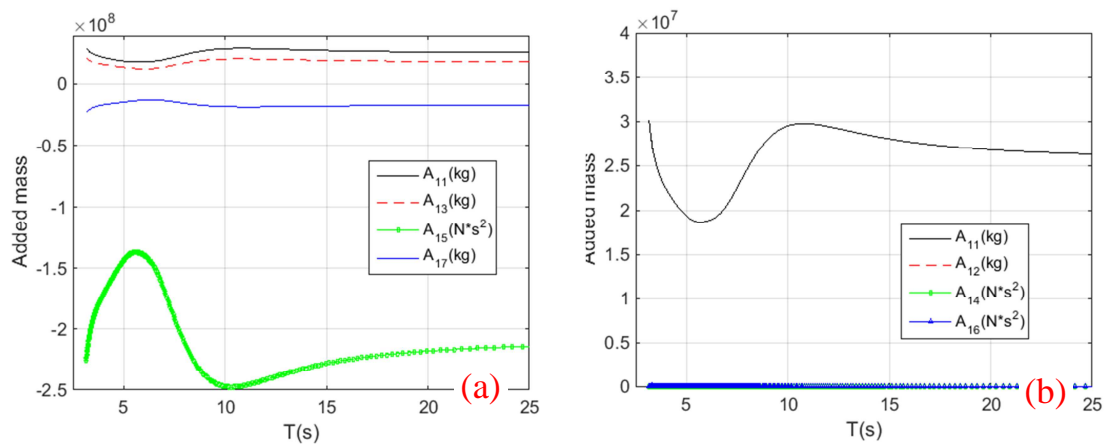
### 250 3.4.2 Cross-radiated added mass and damping coefficients

251 Cross-radiated added masses from other motion modes on surge motion have shown that only the heave  
 252 motions of both structure & piston and the pitch motion would have significant effects since these cross-  
 253 terms (added masses and damping coefficients) have comparable magnitudes (positive or negative) to the  
 254 self-radiated terms (see Figure 6a and Figure 7a), while the sway, roll and yaw motions have little effects  
 255 on the cross-terms to surge (Figure 6b and Figure 7b). Obviously, these motions (surge, heaves and pitch)  
 256 are strongly coupled each other.

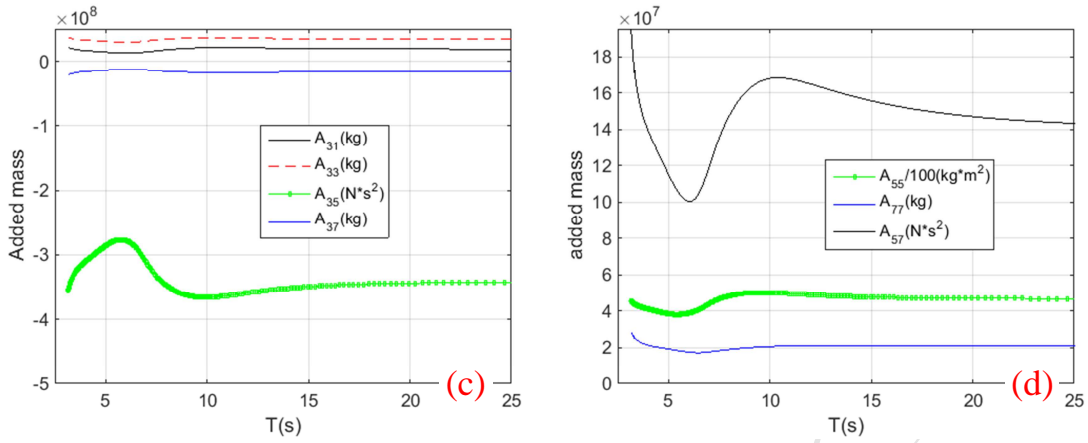
257 It is also seen that the coupling effects can be either positive or negative manner. From the mathematical  
 258 equation, the positive and negative cross-term added masses can be understood as following: a positive  
 259  $A_{13}$  means that an increased heave motion (structure) will cause a decrease in surge motion, and negative  
 260  $A_{15}$  and  $A_{17}$  mean that the increased pitch motion (pitching nose down is positive) and heave motion of  
 261 the piston will induce an increase in the surge motion.

262 Similarly, for the structure heave motion, see Figure 6c and Figure 7c, large coupling effects could come  
 263 from surge, pitch and piston heave. From Figure 6d and Figure 7d, it can be seen that the pitch motion is  
 264 strongly coupled with the piston heave motion.

265 In all, for the RM6 BBDB device, the surge, heave (structure), pitch and the piston heave are all strongly  
 266 coupled, while other motion modes (sway, roll and yaw) are not coupled to these motions. From the point  
 267 of view of wave energy conversion, only surge, heave, pitch (structure) and the heave (piston) will  
 268 contribute.



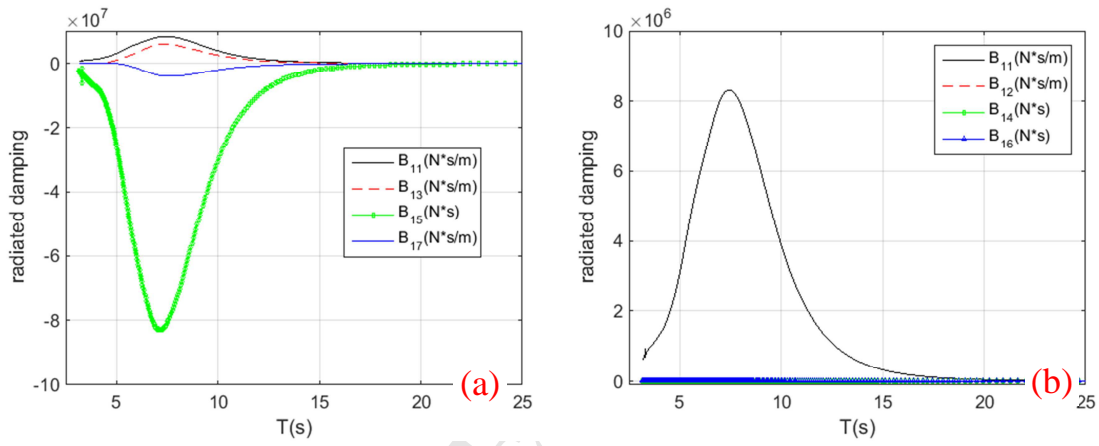
269



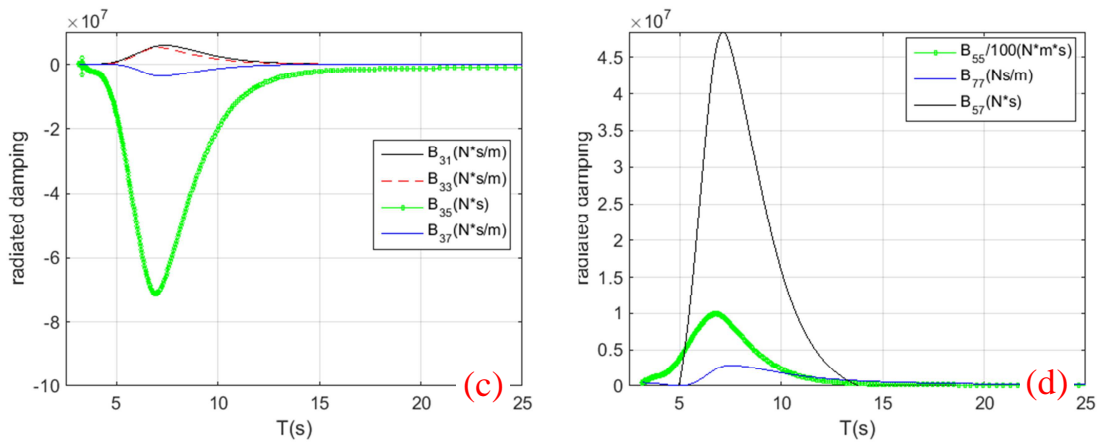
270

271

Figure 6 Cross-radiated added mass/moment of inertia



272



273

274

Figure 7 Cross-radiated damping coefficients



275 **3.5 Decoupled motions**

276 In the numerical modelling, it is possible to study the fully decoupled motions of the structure and the  
 277 piston. This can be done by setting all the cross terms as zeros in the dynamic equation (3), that is,

$$\begin{pmatrix} a_{11} & 0 & 0 & 0 & 0 & 0 & 0 \\ 0 & a_{22} & 0 & 0 & 0 & 0 & 0 \\ 0 & 0 & a_{33} & 0 & 0 & 0 & 0 \\ 0 & 0 & 0 & a_{44} & 0 & 0 & 0 \\ 0 & 0 & 0 & 0 & a_{55} & 0 & 0 \\ 0 & 0 & 0 & 0 & 0 & a_{66} & 0 \\ 0 & 0 & 0 & 0 & 0 & 0 & a_{77} \end{pmatrix} \begin{pmatrix} X_1 \\ X_2 \\ X_3 \\ X_4 \\ X_5 \\ X_6 \\ X_7 \end{pmatrix} = \begin{pmatrix} F_1 \\ F_2 \\ F_3 \\ F_4 \\ F_5 \\ F_6 \\ F_7 \end{pmatrix} \quad (6)$$

278 Principally, the fully de-coupled dynamics can hardly be fully reproduced in physical modelling, because  
 279 in physical modelling, it is possible to limit certain motions. For instance, a mechanism can be used to  
 280 allow only heave motion of the structure (identified as ‘heave only (structure)’) while other motion modes  
 281 are limited. However, for the BBDB OWC device, the heave motion of the water body in the water  
 282 column is always present regardless of the structure motion modes, even for the fixed structure. As such,  
 283 the heave motions of the structure and of the piston will still couple together in reality. One special  
 284 decoupled case in physical modelling is the fixed OWC, in which only the heave motion of the piston is  
 285 allowed, thus it is fully decoupled from all the motion modes of the structure.

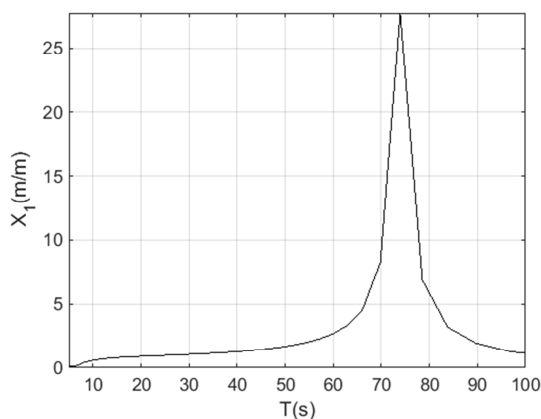
286 In numerical modelling of the decoupled motion analysis, it is easy to fully decouple all the motions, and  
 287 it provides a good way to examine the natural resonance periods for all motion modes, while they may be  
 288 impossible to obtain from physical modelling. Solving Eq. (6) yields the decoupled resonance periods as  
 289 in the following table.

290 Table 2 Motion natural periods using the decoupled method

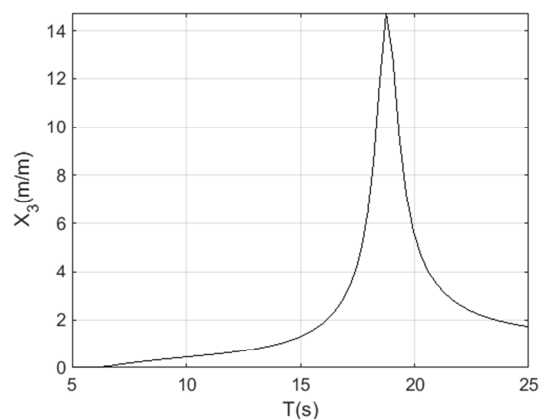
Motion mode	Resonance period (s)	description
Surge	~73.92s	$K_1=200,000$ N/m
Sway	~75.00s	$K_2=200,000$ N/m
Heave	18.76s	Decoupled
Roll	18.76s	Decoupled
Pitch	15.14s	Decoupled
Yaw	~250s	$K_6=2,000,000$ Nm
Piston	13.75s	Fix OWC/decoupled

291 The RAOs for the fully decoupled motions are plotted in *Figure 8*, and it can be seen that these are the  
 292 typical RAOs for the independent motions, with a large peak at the resonance periods. However, if all  
 293 these decoupled RAOs are plotted against the IWS RAO in motion coupling, an interesting comparison  
 294 can be seen in *Figure 9*: 3 peaks in the IWS RAO are corresponding to 3 different periods, i.e., 8.61s,  
 295 12.08s and 16.11s, while are all different from the resonance periods of structure heave (18.76s), pitch  
 296 (15.14s) and the piston heave (13.75). Due to the strong coupling between different motion modes, the  
 297 individual resonances will no longer present directly in the IWS RAO, with its peaks being different from  
 298 the main contributors: the heave (structure), pitch and heave (piston). This is essentially very different  
 299 from the symmetrical OWC as studied in [28]: for an axi-symmetrical spar OWC, its two peaks in IWS  
 300 RAO are directly linked to the resonance of the structure heave and the piston heave motions (they are  
 301 only weakly coupled).

302 Because the strong couplings among the motion modes, especially the surge, heave and pitch (structure)  
 303 and the heave (piston), to get an expected response for the IWS motions (which can be regarded as a good  
 304 indicator for power performance since a high RAO in IWS means a possible high power conversion  
 305 capacity), the optimisation of the BBDB OWC wave energy converter needs a systematic approach, rather  
 306 than a simple adjustment of one individual resonance periods. In this research (including the second part),  
 307 a systematic approach will be carried out to optimise the device design so a better hydrodynamic and thus  
 308 power performance may be achieved using the optimisation approaches.



(a) Surge RAO: ~73.92s



(b) Heave RAO (structure): 18.76s

309  
 310

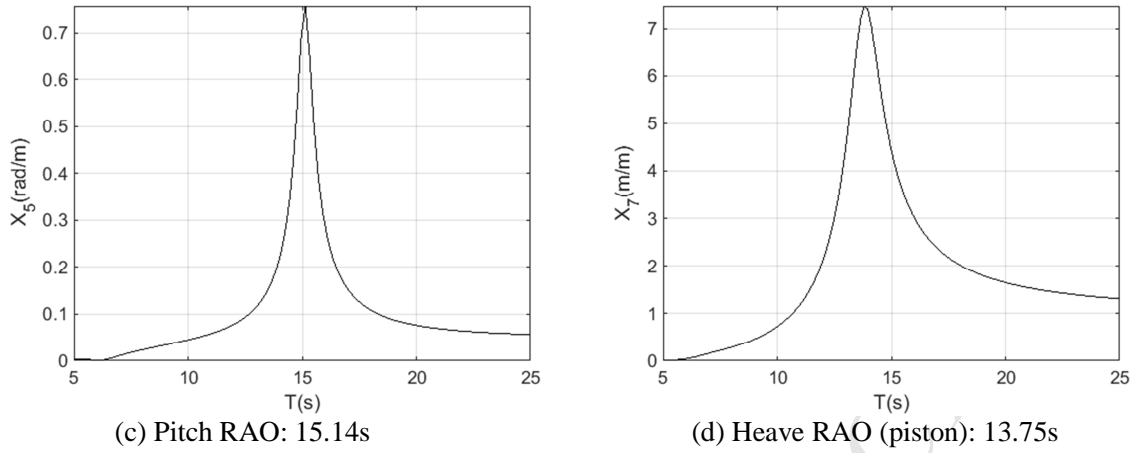


Figure 8 RAOs of the decoupled motions in waves (with the linear viscous damping)

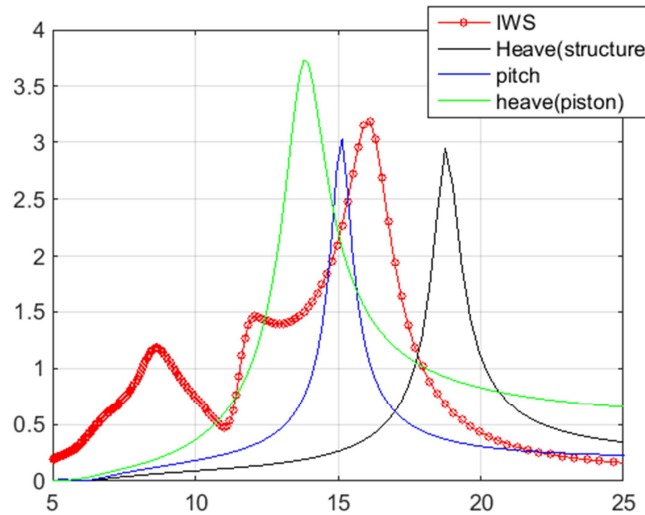
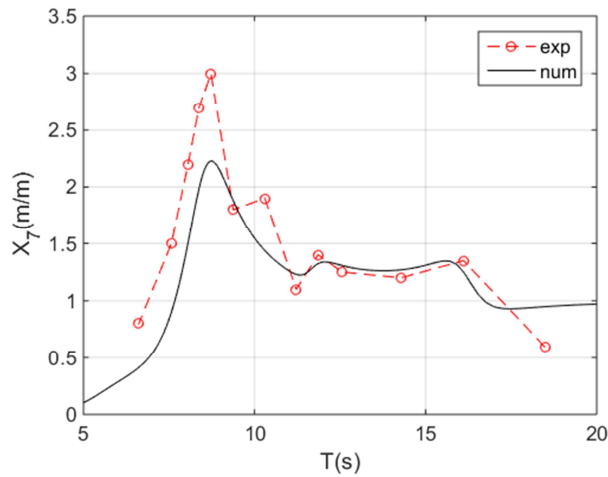


Figure 9 IWS RAO against decoupled RAOs of the relevant motion modes (all with viscosity). Note: the decoupled RAOs have been scaled for comparison: heave (structure)\*0.2; pitch\*4; heave (piston)\*0.5

## 4 VALIDATION

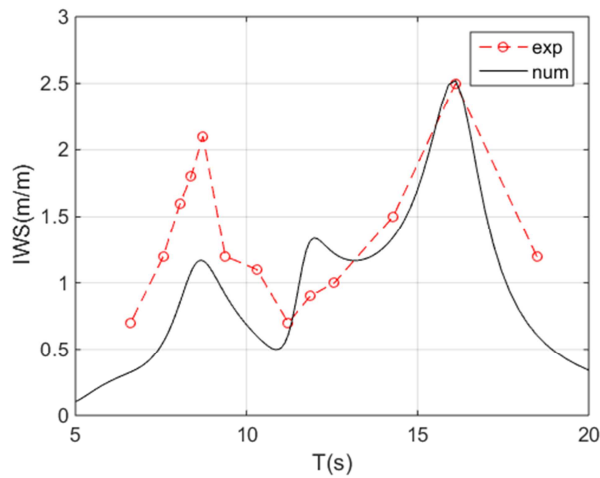
To validate the numerical method schemed in the previous sections, the responses of the water body motion and the IWS motion from the numerical modelling are compared to the experimental data (the experimental data are taken from Ref. [23]). Figure 10 and Figure 11 give the comparisons of the water body (piston) motion and the IWS motion, i.e., the relative heave motion between the water body and the structure, respectively. The numerical modelling results agree quite well with the experimental data. From the comparisons, it can be seen that the main features of the RAOs of the piston heave motion and the internal water surface (IWS) motion are both well predicted, though the peak values may not be well

325 predicted in the numerical modelling. Considering the general linear viscous damping coefficients using  
 326 Eq. (5), the RAOs of the piston heave motion and the IWS motion are both slightly over damped. But as a  
 327 generic formulation, Eq. (5) is still considered to be a good generic expression.



328

329 *Figure 10 Water body motion RAOs (comparison of numerical modelling and physical model test data)*



330

331 *Figure 11 IWS motions in the BBDB RM6 wave energy converter*

## 332 **5 MOTION COMPARISONS AND OPTIMISATIONS**

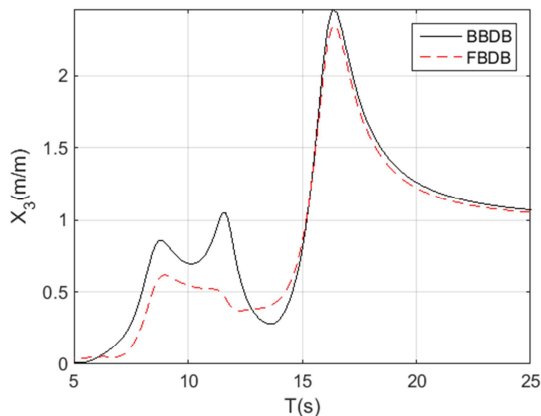
333 In this section, motion RAO comparisons will be made for different scenarios, including different device  
 334 orientations, duct lengths, water column sizes and mooring stiffness. The comparisons will be made for  
 335 the motions of structure surge, heave and pitch and of the piston heave, with special attention to the  
 336 motion of the internal water surface (IWS), which is the most important factor for wave energy

337 conversion for the BBDB OWC devices (more details can be found in the second part of the research  
338 [38]).

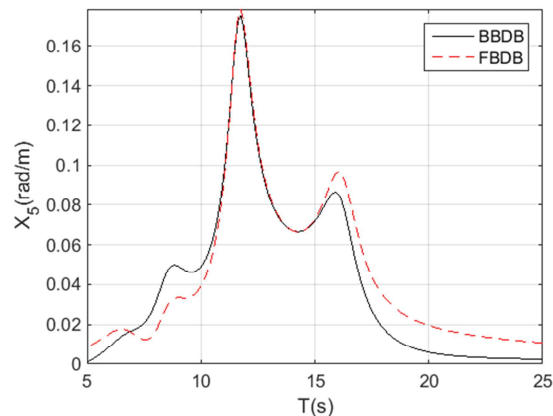
### 339 5.1 BBDB and FBDB

340 An interesting factor is the orientation of the bent duct buoy. From all the experience and the relevant  
341 research work, the backward bent duct buoy (i.e., 'BBDB') is proposed because this is the orientation the  
342 bent-duct OWC device is most efficient (see the wave direction for BBDB in *Figure 2*). Here a  
343 comparison is made to the forward bent duct buoy ('FBDB'), for which the wave comes to the duct  
344 opening, i.e, the BBDB and FBDB are orientated in waves in  $180^\circ$  difference. *Figure 12* shows the  
345 comparisons for different motion modes. For the heave motions of the structure, small heave RAOs can  
346 be seen for the waves with periods of 5-15s for FBDB (*Figure 12a*). For the pitch motions, again small  
347 difference in RAOs can be seen at both small and large wave periods, while there is no significant  
348 difference for wave periods between 10s and 15s (*Figure 12b*). For the heave motion of the piston, large  
349 deficits in RAO happen in the wave periods of 5s to 10s for FBDB, especially the piston heave RAO for  
350 FBDB is very small at the wave periods from 5-7.5s. When the wave period is larger than 10s, these two  
351 orientations have very close RAOs.

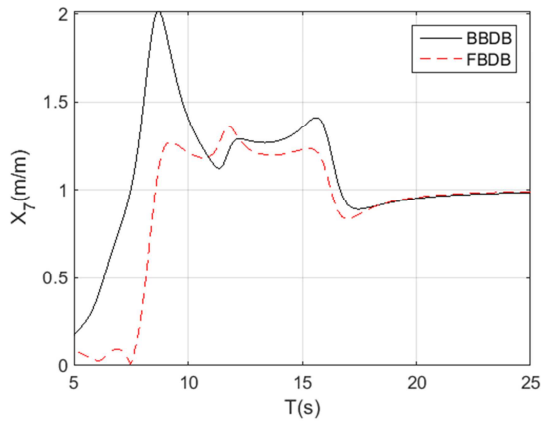
352 Under the strong coupling of above motions, the IWS motions shows a complicated combination (*Figure*  
353 *12d*). The BBDB IWS RAO is larger than the FBDB IWS RAO, except the wave periods between 10s and  
354 12s for which the FBDB IWS RAO is slightly larger than that of BBDB. The largest difference in the  
355 RAOs is in the wave periods below 8s, where the FBDB has very small IWS RAOs, which could be a  
356 worst IWS RAO in terms of wave energy conversion (details can be seen in the second part of the  
357 research).



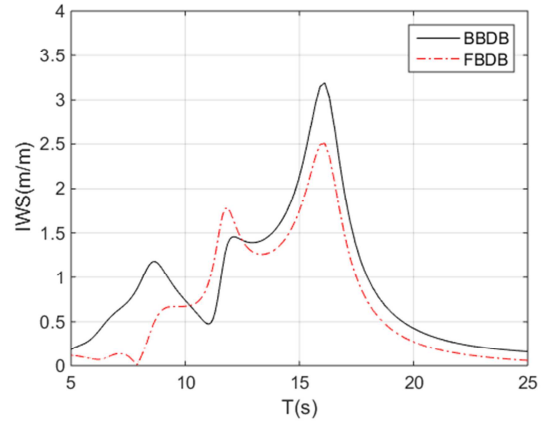
358 (a) Heave RAOs (structure)



359 (b) Pitch RAOs



(c) Heave RAO (piston)



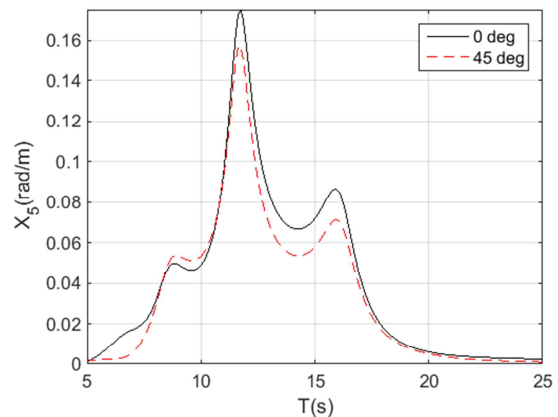
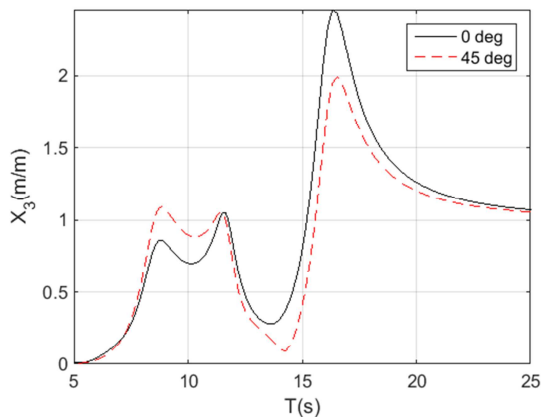
(d) IWS RAO

Figure 12 RAO comparison for BBDB and FBDB

## 5.2 Effect of wave angles

It is well known that the BBDB OWC device has a highest energy conversion efficiency when the incoming waves head to the back of the BBDB device. Hence, the BBDB devices are generally deployed heading to the dominant wave direction at the site. However, in reality, waves may propagate to the device in different directions. Following example is a comparison of the motions of the device in head waves and in  $45^\circ$  waves. For the heave motion of the structure, large difference can be seen near the peaks and troughs (Figure 13a) while relatively smaller difference can be found in the heave motion of the piston (Figure 13c). For the pitch motion (Figure 13b), some difference can be seen, with the pitch RAO for FBDB having smaller magnitude.

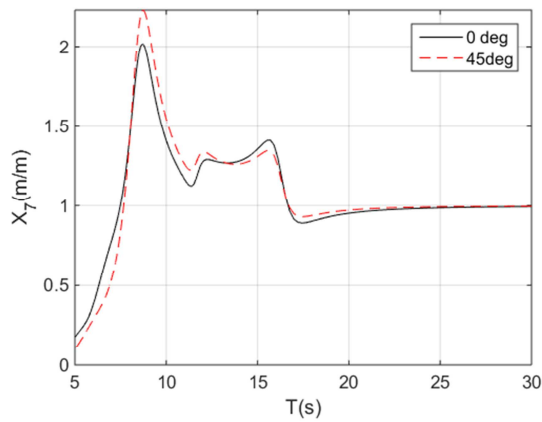
From Figure 13d, it can be seen that the IWS RAO in  $45^\circ$  waves is smaller than that in the head waves, which is an indicator that the device is less efficient in  $45^\circ$  waves than in head waves.



374

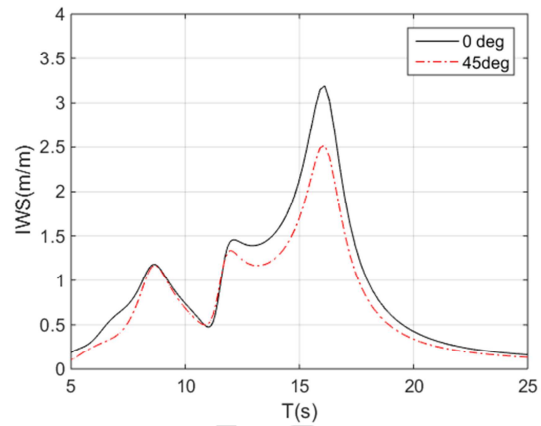
375

(a) Heave RAOs (structure)



376

(b) Pitch RAOs



377

(c) Heave RAO (piston)

(d) IWS RAO

378

Figure 13 RAO comparisons in head wave and in waves of 45°

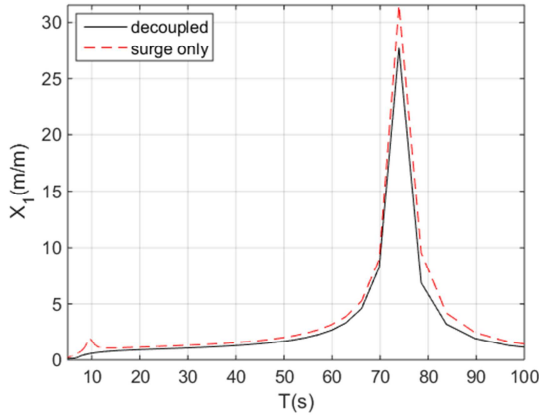
### 379 5.3 Cases with limited motions

380 In the section, attention is paid to the cases of limited/isolated motions, the cases that the structure  
 381 motions are limited to the given motion mode. For instance, 'surge only' means the device structure can  
 382 only move in surge whilst all other motion modes (structure) are set to zeros. The same methods are  
 383 applied for heave and pitch only, in which the structure heave and pitch are only allowed. A very special  
 384 case is the case with a fixed structure ('fix'), which means the device structure is fixed, hence no structure  
 385 motions are allowed.

386 It must be noted that such isolated motion scenarios, the water body in the water column will not be  
 387 limited, hence the heave motion of the piston is allowed in all the isolated cases. Also, it will be seen in  
 388 the flowing comparisons that the heave motion of the piston is always strongly coupled with the given  
 389 motion mode of the structure.

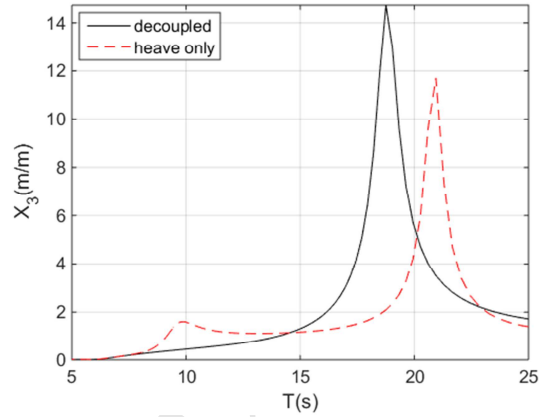
390 All comparisons are made for the allowed motions against the decoupled motions (from Eq. (6)). As a  
 391 decoupled motion in mathematics, it is fully isolated from effect or coupling from other motion modes.  
 392 Figure 14 shows the comparisons of the isolated motion and the decoupled motion. Due to the coupling of  
 393 the isolated motions with the water body in the water column, the heave and pitch motions in their  
 394 motion-isolated cases are very different from the decoupled motions, with RAO peaks happening at  
 395 different wave periods (see Figure 14b and Figure 14c) while the surge motion has different in the peak in  
 396 the RAOs, and there is a small peak in the surge only for the wave at period of 10s (Figure 14a), which is  
 397 actually caused by the coupling of the surge and the water body in the water column.

398 In the fixed case, the water body motion is fully isolated from any other motion modes of the structure  
 399 physically, hence it is exactly as in same condition as the decoupled case for the heave motion of the  
 400 piston. As a result of this, these two RAOs are identical (Figure 14d).



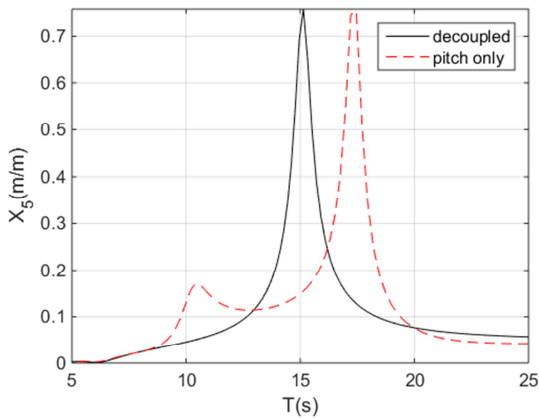
401

(a) Decoupled surge and surge only



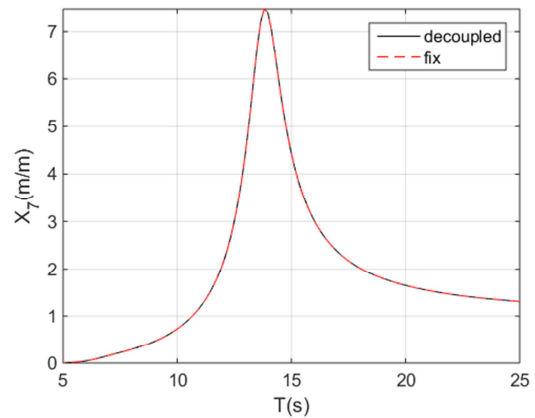
402

(b) Decoupled heave and heave (structure) only



403

(c) Decoupled pitch and pitch only



404

(d) Decoupled heave (piston) and fix device

405

Figure 14 RAO comparisons of the decoupled and isolated motions

#### 406 5.4 Effect of horizontal duct lengths

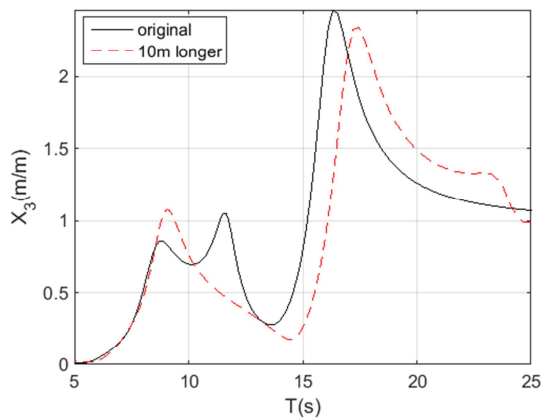
407 Duct length of the BBDB devices have large effects on the motions of the device (and eventually to the  
 408 energy conversion efficiency). The following case is the comparison of the motion RAOs for the devices  
 409 with different duct lengths. For a fair and simple comparison, all the device parameters (such as the centre  
 410 of gravity, the displacement, the moment of inertia) are kept unchanged and achievable. Hence the  
 411 differences are mostly caused due to the added mass and damping coefficients as well as the excitation  
 412 forces on the structure and the water body in the water column.



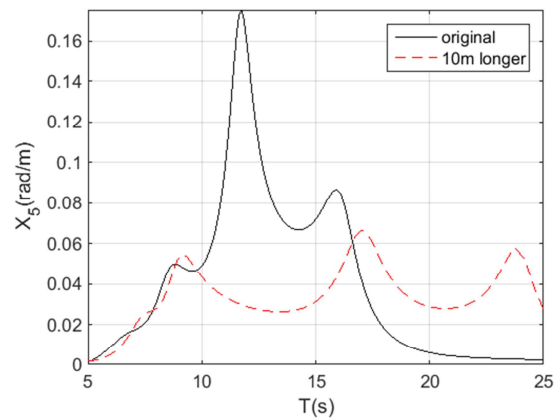
413 Figure 15 shows the comparisons of the motion RAOs for two different duct lengths. The original design  
 414 is same as the RM6 [23, 28], which has an overall duct length of 35m, and a longer duct ('10m longer')  
 415 means the duct length is 10m longer, i.e, the overall duct length is 45m. Due to the change in duct length,  
 416 the motion RAOs are changed. For the heave RAO (structure), two peaks can be seen, rather than 3 peaks  
 417 in the original design, with peaks happening at a slightly larger wave periods (Figure 15a). Obviously, the  
 418 largest difference is seen for the pitch motions (Figure 15b). The RAO change in pitch is dramatic, in  
 419 which 3 peaks are more evenly distributed, including the peak values, whilst in the original design, the  
 420 pitch has a dominant response in the wave period of 12s.

421 The heave motion (piston) has changed, similarly to the heave motion of the structure. Again, the peaks  
 422 can be seen happening at the slightly larger wave periods for the longer duct (Figure 15c).

423 An interesting result can be seen of the IWS motions (Figure 15d). With a longer duct, the RAO is  
 424 smoother than the original design. Unlike the original design, where there is a deficit at the wave period  
 425 of 11s (this is very unfavourable for wave energy conversion, see [28]), the device with a longer duct does  
 426 not have such a deficit, hence it is beneficial for improving wave energy conversion.



427  
 428 (a) Heave RAOs (structure)



(b) Pitch RAOs

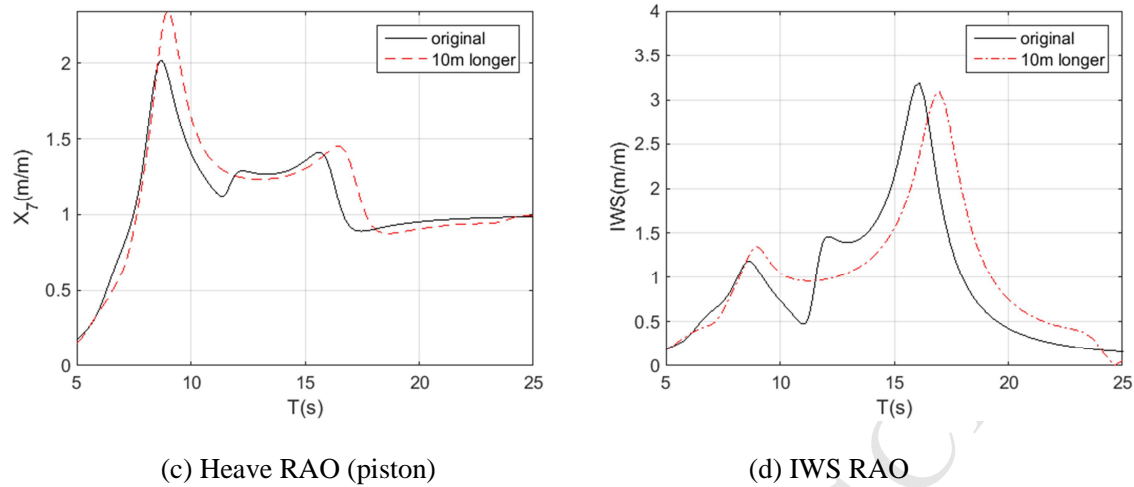
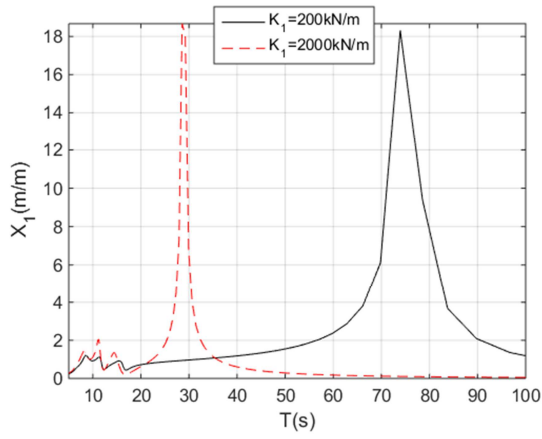


Figure 15 RAO comparisons of the original BBDB and longer BBDB

### 5.5 Effect of mooring stiffness

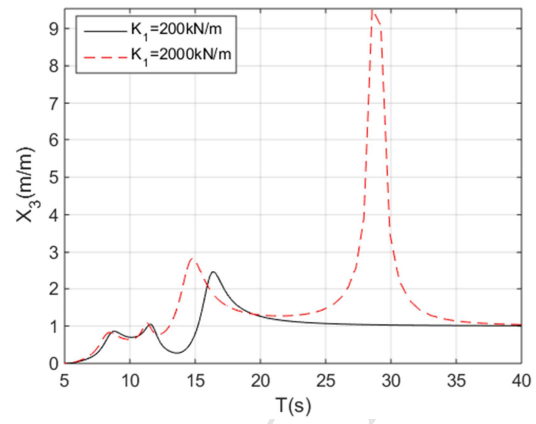
An interesting finding in the numerical modelling is the effect of the mooring stiffness on the motions. Conventionally, mooring system is designed to confine the device within a pre-defined profile and hence the device can only move with a limited excursion, even in the extreme wave conditions. For such a purpose, the conventional mooring may have a relatively small stiffness, thus its resonance periods for surge, sway and yaw motions are quite large (normally more than 60s, and in this case, about 74s) to avoid the resonance in the energetic waves. However, as a case study here, the mooring stiffness is increased 10 times (from 200 kN/m to 2000 kN/m), the surge resonance period is changed from 74s to 29s (Figure 16a). Since the coupling among the surge motion to other motion modes, the heave motions (structure and piston both) and pitch motion are all affected (Figure 16b-d), with a significant change on pitch motion (Figure 16c) even at small wave periods. When a larger mooring stiffness is applied, the IWS RAO has changed accordingly (Figure 16e). With a stiffer mooring, it is possible to improve the motion performance for the wave periods less than 15s, for which most interested waves are included for wave energy conversion. Hence it is possible to improve the BBDB device power performance using a stiffer mooring.



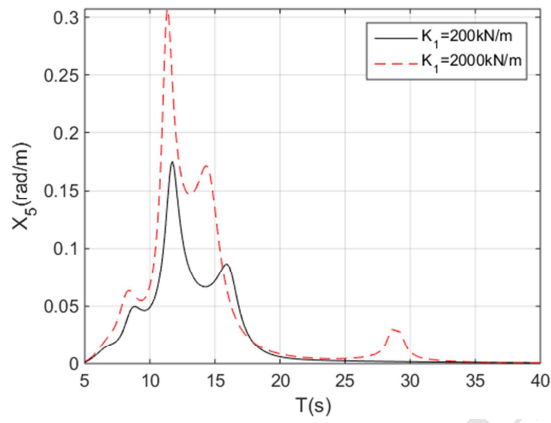
447

448

(a) Surge RAOs



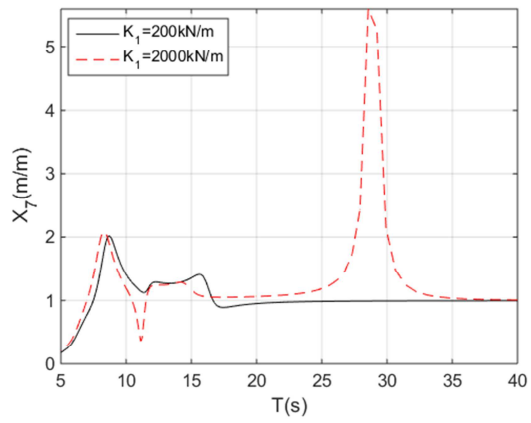
(b) heave RAOs (structure)



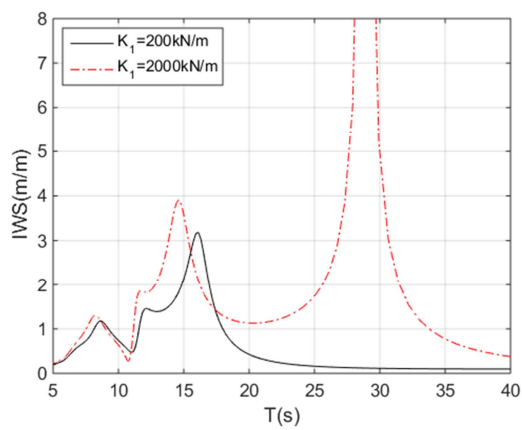
449

450

(c) pitch RAOs



(d) heave RAOs (piston)



451

452

(e) IWS RAOs

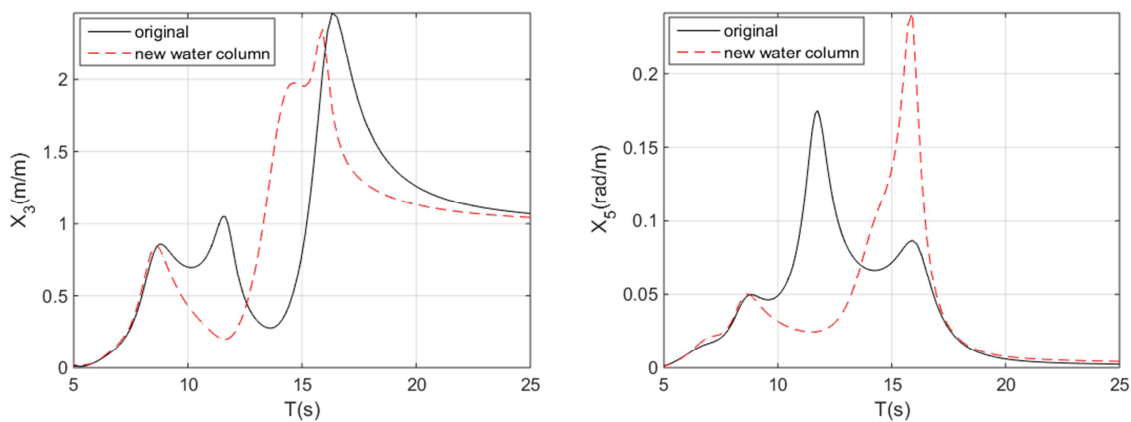
453

Figure 16 RAO comparisons of the different mooring stiffness

## 454 5.6 Modification of vertical water column

455 In the original design of RM6, the vertical water column has a larger area ( $17.5\text{m}\times 27\text{m}$ ) than that of the  
 456 horizontal column ( $14\text{m}\times 27\text{m}$ ). In a modification of the design, a study is made to the modified vertical  
 457 column size, so the vertical water column has a same size as that of horizontal water column ( $14\text{m}\times 27\text{m}$ ,  
 458 'new water column'). The motion comparisons are seen in Figure 17. As a simple purpose for the uniform  
 459 water column, it is to avoid the fluid being accelerated or decelerated when the flow move in the different  
 460 size of the water column. However, the hydrodynamic changes are much more than the accelerated or  
 461 decelerated flow. Due to the change of the vertical water column, significant changes can be seen in the  
 462 structure heave and pitch RAOs (Figure 17a & b). Relatively, the change for the piston heave RAO is less  
 463 dramatic, however, a much enlarged peak can be seen at the wave period of about 8s (Figure 17c).

464 As a result of the change, the IWS RAO shows very a good increase for the wave period less than 15s,  
 465 and the largest benefit would be the removal of the deficit in the IWS RAO as shown in the original  
 466 design (Figure 17d), though the modification may lead to less efficient for longer wave (more than 15s).  
 467 Since we are not very interested in long waves (its occurrence is low), it can be expected that the changed  
 468 water column may be very beneficial for improving wave energy extraction from seas.

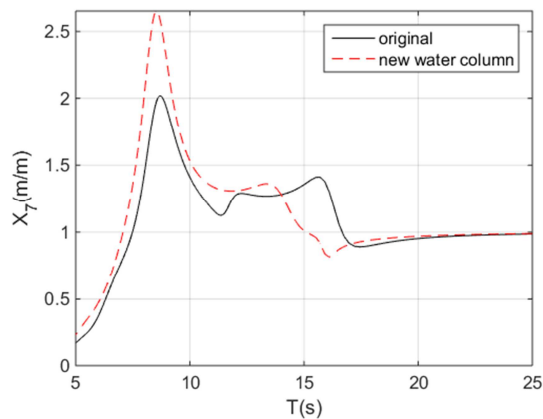


469

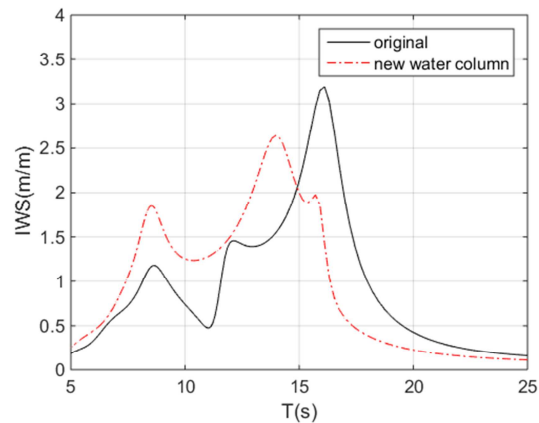
470

(a) Heave RAOs (structure)

(b) Pitch RAOs



(c) Heave RAO (piston)



(d) IWS RAO

Figure 17 RAO comparisons of the original water column and the new water column (uniform)

## 6 CONCLUSIONS

The backward bent duct buoy (BBDB) oscillating water column wave energy converters are very promising wave energy converters because of their unique features using multiple motion modes to enhance its power performance. This research provides the methods for hydrodynamic analysis and thus for optimising the BBDB OWC wave energy converters so for maximising wave energy conversion for the BBDB OWC wave energy converters. From the study, following conclusions can be drawn:

- Due to the non-symmetry of the BBDB OWC devices, the motions of the structure surge, heave and pitch and of the 'piston' heave are all strongly coupled, and these motions must be solved in a coupled manner so for studying the hydrodynamic performance (the energy conversion as well) of the BBDB devices.
- The internal water surface (IWS) motions is essentially a result of the strong couplings among these motions. Individual resonance periods from the de-coupled model can be very different from those shown in the coupled responses. Hence a change of one individual resonance period may induce some complicated results. As such, the optimisations must be carried out in a systematic manner.
- It has been shown that the backward bent duct would have much better hydrodynamic performance (thus the power performance) than the forward bent duct in terms of hydrodynamic performance in the wave periods of 5-10s (which cover the main waves for wave energy conversion). When waves come from a different direction (for instance 45°), a reduction of the hydrodynamic performance (mainly on IWS response) would be expected.

- 493 - Longer horizontal duct could significantly improve the hydrodynamic performance in terms of wave  
 494 energy conversion in the case of RM6 design.
- 495 - Using a uniform size of the water column may improve the hydrodynamic response, especially the  
 496 removal of the deficit in the IWS response (around 11s). This can be regarded as an indicator of a  
 497 better power performance for the device.
- 498 - Mooring system could be an effective factor for improving wave energy conversion, since it is  
 499 possible to use a stiffer mooring to increase the hydrodynamic performance of the BBDB device for  
 500 the purpose of wave energy conversion.

## 501 ACKNOWLEDGEMENTS

502 The author would like to thank the friends and the former colleagues and friends for their help when I was  
 503 with MaREI, University College Cork, Ireland.

## 504 REFERENCES

- 505 1. EC, *Study on lessons for ocean energy development*, 2016, cited at: [http://publications.europa.eu/resource/ellar/3a4f6411-6777-11e7-b2f2-01aa75ed71a1.0001.01/DOC\\_1](http://publications.europa.eu/resource/ellar/3a4f6411-6777-11e7-b2f2-01aa75ed71a1.0001.01/DOC_1)
- 506 507 2. Magagna, D., R. Monfardini, and A. Uihleih, *JRC Ocean Energy Status Report 2016 Edition: Technology, market and economic aspects of ocean energy in Europe*, 2016, cited at: [https://setis.ec.europa.eu/sites/default/files/reports/ocean\\_energy\\_report\\_2016.pdf](https://setis.ec.europa.eu/sites/default/files/reports/ocean_energy_report_2016.pdf) (11/12/2017)
- 508 509 3. Falcao, A., 2010. Wave energy utilization: a review of the technologies. *Renewable and Sustainable Energy Reviews*, **14**(3): pp. 899-918. doi: 10.1016/j.rser.2009.11.003.
- 510 511 4. Masuda, Y., et al. 1988, The backward bend duct buoy-an improved floating type wave power device. *Proceedings of OCEANS '88. A Partnership of Marine Interests*. 31 Oct-2 Nov. 1988. Baltimore, USA.
- 512 513 5. Ross, D., *Power from sea waves*. 1995: Oxford University Press.
- 514 515 6. Evans, D.V., 1978. The oscillating water column wave-energy device. *IMA Journal of Applied Mathematics*, **22**(4): pp. 423-433. doi: 10.1093/imamat/22.4.423.
- 516 517 7. Masuda, Y. 1979, Experimental full-scale results of wave power machine Kaimei in 1978. *Proceedings of the 1st Symposium on Wave Energy Utilization*,. 30 Oct.-1st Nov. 1979. Gothenburg, Sweden.
- 518 519 8. Evans, D.V. and R. Porter, 1995. Hydrodynamic characteristics of an oscillating water column device. *Applied Ocean Research*, **17**(3): pp. 155-164. doi: 10.1016/0141-1187(95)00008-9.
- 520 521 9. Sheng, W. and A. Lewis, 2016. Wave energy conversion of oscillating water column devices including air compressibility. *Journal of Renewable and Sustainable Energy*, **8**: pp. 054501. doi: 10.1063/1.4963237.
- 522 523 10. O'Sullivan, D.L. and A. Lewis, 2010. Generator selection and comparative performance in offshore oscillating water column ocean wave energy converters. *IEEE Transactions on Energy Conversion*, **26**(2): pp. 603-614. doi: 10.1109/TEC.2010.2093527.
- 524 525 11. Folley, M., R. Curran, and T. Whittaker, 2006. Comparison of LIMPET contra-rotating wells turbine with theoretical and model test predictions. *Ocean Engineering*, **33**(8-9): pp. 1056-1069. doi: 10.1016/j.oceaneng.2005.08.001.
- 526 527 12. Boake, C., T. Whittaker, and M. Folley. 2002, Overview and initial operational experience of the LIMPET wave energy plant. *Proceedings of The Twelfth (2002) International Offshore and Polar Engineering Conference*. May 26-31, 2002. Kitakyushu, Japan.
- 528 529 13. Le Crom, I., et al. 2009, Numerical Estimation of Incident Wave Parameters Based on the Air Pressure Measurements in Pico OWC Plant *Proceedings of the 8th European Wave and Tidal Energy Conference*. 7-10 Sep. 2009. Uppsala, Sweden.
- 530 531 14. Neumann, F. and I. Le Crom. 2011, Pico OWC - the Frog Prince of Wave Energy? Recent autonomous operational experience and plans for an open real-sea test centre in semi-controlled environment. *Proceedings of the 9th European Wave and Tidal Energy Conference*. 5-9 Sep. 2011. Southampton, UK.
- 532 533 534 535

- 536 15. Henriques, J.C.C., et al. 2017, A comparison of biradial and Wells air turbines on the Mutriku breakwater OWC wave power  
537 plant. *Proceedings of the ASME 2017 36th International Conference on Ocean, Offshore and Arctic Engineering*. June 25-30,  
538 2017., Trondheim, Norway.
- 539 16. Torre-Enciso, Y., et al. 2009, Mutriku Wave Power Plant: from the thinking out to the reality. *Proceedings of the 8th*  
540 *European Wave and Tidal Energy Conference*. 7-10th Sep. 2009. Uppsala, Sweden.
- 541 17. Alcorn, R., M. Healy, and A.W. Lewis. 2012, Lessons learned from the Galway bay Seatrials of the EU funded CORES  
542 project. *Proceedings of the 4 International Conference on Ocean Energy*. 17-19 Oct. 2012. Dublin, Ireland.
- 543 18. OceanEnergy, *Ocean Energy: A World of Power*, 2015, cited at: <http://www.oceanenergy.ie/> (15/10/2017)
- 544 19. Heath, T., 2012. A review of oscillating water columns. *Philosophical Transactions of the Royal Society A: Mathematical,*  
545 *Physical & Engineering Sciences*, **370**: pp. 235-245. doi: 10.1098/rsta.2011.0164.
- 546 20. Mavrakos, S.A. and D.N. Konispoliatis. 2012, Hydrodynamic analysis of a vertical axisymmetric oscillating water column  
547 device floating in finite depth waters. *Proceedings of the ASME 31st International Conference on Ocean, Offshore and*  
548 *Arctic Engineering*. July 1-6, 2012. Rio de Janeiro, Brazil.
- 549 21. Evans, D.V., 1982. Wave-power absorption by systems of oscillating surface pressure distributions. *Journal of Fluid*  
550 *Mechanics*, **114**: pp. 481-499. doi: 10.1017/S0022112082000263.
- 551 22. Babarit, A., et al., 2011, Numerical estimation of energy delivery from a selection of wave energy converters, Final Report,  
552 Ecole Centrale de Nantes & Norges Teknisk-Naturvitenskapelige Universitet. Cited at:
- 553 23. Bull, D., et al., 2014, reference Model 6 (RM6): Oscillating wave energy converter, SANDIA2014-18311, Sandia National  
554 Laboratory. Cited at:
- 555 24. Lopez, I., et al., 2016. Holistic performance analysis and turbine-induced damping for an OWC wave energy converter.  
556 *Renewable Energy*, **85**: pp. 1155-1163. doi: 10.1016/j.renene.2015.07.075.
- 557 25. Lee, C.H. and F.G. Nielsen. 1996, Analysis of oscillating-water-column device using a panel method. *International*  
558 *Workshop on Water Wave and Floating Bodies*. 17-20, Mar. 1996. Hamburg, Germany.
- 559 26. Falcao, A., J.C.C. Henriques, and J.J. Candido, 2012. Dynamic and optimization of the OWC spar buoy wave energy  
560 converter. *Renewable Energy*, **48**: pp. 369-381. doi: 10.1016/j.renene.2012.05.009.
- 561 27. Sheng, W., R. Alcorn, and A.W. Lewis, 2014. Assessment of primary wave energy conversions of oscillating water columns.  
562 II. Power take-off and validations. *Journal of Renewable and Sustainable Energy*, **6**: pp. 053114. doi: 10.1063/1.4896851.
- 563 28. Bull, D., 2015. An improved understanding of the natural resonances of moonpools contained within floating rigid-bodies:  
564 Theory and application to oscillating water column devices. *Ocean Engineering*, **108**: pp. 799-812. doi:  
565 10.1016/j.oceaneng.2015.07.007.
- 566 29. Kurniawan, A., J. Hals, and T. Moan. 2011, Modelling and simulation of a floating oscillating water column. *Proceedings of*  
567 *the ASME 2011 30th International Conference on Ocean, Offshore and Arctic Engineering*. June 19-24, 2011. Rotterdam,  
568 The Netherlands.
- 569 30. Falnes, J., *Ocean Waves and Oscillating Systems: Linear Interaction Including Wave-Energy Extraction*. 2002: Cambridge  
570 University Press.
- 571 31. Nagata, S., et al. 2011, Frequency domain analysis on primary conversion efficiency of a floating OWC-type wave energy  
572 converter 'Backward bent Duct Buoy'. *Proceedings of the 9th European Wave and Tidal Energy Conference*. 5-9 Sep, 2011.  
573 Southampton, UK.
- 574 32. Lewis, A., T. Gilbaud, and B. Holmes. 2003, Modelling the Backward Bent Duct Device-B2D2, a comparison between  
575 physical and numerical models. *Proceedings of 5th European Wave Energy Conference*. 17-20th, Sep. 2003. Cork, Ireland.
- 576 33. Hong, D.C., S.Y. Hong, and S.W. Hong, 2004. Numerical study on the reverse drift force of floating BBDB wave energy  
577 absorbers. *Ocean Engineering*, **31**(10): pp. 1257-1294. doi: 10.1016/j.oceaneng.2003.12.007.
- 578 34. SNL, *Reference Model Project (RMP)*, 2017, cited at: [http://energy.sandia.gov/energy/renewable-energy/water-](http://energy.sandia.gov/energy/renewable-energy/water-power/technology-development/reference-model-project-rmp/)  
579 [power/technology-development/reference-model-project-rmp/](http://energy.sandia.gov/energy/renewable-energy/water-power/technology-development/reference-model-project-rmp/) (10/02/2018)
- 580 35. Neary, V.S., et al., 2014, Methodology for Design and Economic Analysis of Marine Energy Conversion (MEC)  
581 Technologies, SAND2014-9040, Sandia National Laboratories, USA. Cited at:
- 582 36. WAMIT, *User Manual*, 2016, cited at: <http://www.wamit.com/manual.htm> (20/01/2016)
- 583 37. Newman, J.N., *Marine Hydrodynamics*. 1977: The MIT Press, Cambridge, Massachusetts, USA.
- 584 38. Sheng, W., 2018. Motion and performance of BBDB OWC wave energy converters: II, Power conversion. *Prepared for*  
585 *journal publication*.

586

## Highlights:

- Formulate the Hydrodynamic equation for BBDB oscillating water column wave energy converters.
- Provide the decoupled hydrodynamic model for further understanding of the coupling between motions.
- Perform the analyses of hydrodynamic performance of the BBDB device.
- Optimise the BBDB device for better hydrodynamic performance.